CrossMark

Hydrogen Molecules in the Dark Ages Halos: Thermal Emission versus Resonant Scattering

B. Novosyadlyj[1,2], V. Shulga[1,3] , Yu. Kulinich[2], and W. Han[1]

[1] College of Physics and International Center of Future Science of Jilin University, Qianjin Street 2699, Changchun, 130012, People's Republic of China
[2] Astronomical Observatory of Ivan Franko National University of Lviv, Kyryla i Methodia str., 8, Lviv, 79005, Ukraine
[3] Institute of Radio Astronomy of NASU, 4 Mystetstv str., 61002 Kharkiv, Ukraine

Abstract

The emission from dark ages halos in the lines of transitions between the lowest rotational levels of hydrogen and hydrogen deuteride molecules is analyzed. It is assumed that molecules are excited by the cosmic microwave background (CMB) and collisions with hydrogen atoms. The physical parameters of halos and the number density of molecules are precalculated assuming that halos are homogeneous top-hat spheres formed from the cosmological density perturbations in the four-component universe with post-Planck cosmological parameters. The differential brightness temperatures and differential spectral fluxes in the rotational lines of H_2–HD molecules are computed for two phenomena: thermal luminescence and resonant scattering of CMB radiation. The results show that the expected maximal values of differential brightness temperature of warm halos ($T_K \sim 200$–800 K) are at the level of nanokelvins, are comparable for both phenomena, and are below the sensitivity of modern submillimeter radio telescopes. For hot halos ($T_K \sim 2000$–5000 K) the thermal emission of H_2-ortho molecules dominates and the differential brightness temperatures are predicted to be of a few microkelvins at the frequencies 300–600 GHz, which could be detectable with next-generation telescopes.

Key words: cosmology: theory – galaxies: formation – galaxies: high-redshift – hydrodynamics – intergalactic medium – stars: formation

Supporting material: animations

1. Introduction

The formation of the first luminous objects of the universe is an important topic in current cosmology. The generally accepted paradigm is that they are formed from the initial small matter density and velocity perturbations generated at the early stages of the evolution of the universe. The most interesting stages of their early evolution are hidden in the Dark Ages, a period between the last scattering of the cosmic microwave background (CMB) at $z \approx 1000$ and reionization of the intergalactic medium by early luminous objects at $z \approx 10$ (Planck Collaboration et al. 2018b). The theories of generation and evolution of cosmological perturbations successfully describe the observed anisotropy of CMB and the large-scale structure of the universe that make it possible to evaluate the basic parameters of the cosmological model of the universe and the ratio of the densities of its main components such as baryonic matter, dark matter, and dark energy with sufficient accuracy. The lowest scales in these theories, which are probed by observations, are dozens of megaparsecs in current astronomical units that are essentially larger than expected ones for the first luminous objects, stars, globular clusters, or dwarf galaxies. Numerical simulations of the large-scale structure formation at these scales are very complicated and ambiguous because the nonlinear dynamical effects in the multicomponent medium, gas dynamics, molecular chemistry, and cooling/heating processes become important or even key. The considerable ambiguity of the predictions of theoretical simulations at these scales is due also to the uncertainty of the physical nature of dark matter and dark energy. This supports the importance of analyzing the possibility of detecting signals from the Dark Ages both in the 21 cm atomic hydrogen line and in the lines of the first molecules.

Theoretical investigations of the possible signal from the Dark Ages in the hyperfine structure 21 cm of atomic hydrogen line are intensive and already have an extensive history (see, for example, reviews Barkana & Loeb 2001; Fan et al. 2006; Furlanetto et al. 2006; Pritchard & Loeb 2012). It was predicted that an expected signal at ~100 MHz can be at the level of hundreds—dozens of millikelvins of brightness temperature. It seems that the long-term efforts of several scientific groups to detect such a signal from the Dark Ages gave the first results: the team of the Experiment to Detect the Global EoR Signature[4] (EDGES) announced the registration of the 21 cm atomic hydrogen absorption line with a brightness temperature of about 0.5 K at $z = 15$–20 (Bowman et al. 2018). Unfortunately, the signal in the molecular lines is expected to be rather weaker but it can be more informative because it can say about molecular chemistry and physical conditions of excitation of lines. The upper limits for such a signal at the level of a few millikelvins have been obtained in a few observations by the IRAM 30 m telescope (de Bernardis et al. 1993), RATAN-600 (Gosachinskij et al. 2002), and the *Odin* satellite (Persson et al. 2010).

The molecular line signals from the Dark Ages can be observed in emission or absorption on the background of the CMB radiation, which is defined by competition of excitation/de-excitation of levels by the CMB radiation and the local sources of radiation or collisions with particles. So, the local physics conditions in the baryonic matter of the Dark Ages may cause secondary anisotropy of the CMB. This mechanism is known as thermal emission/absorption and it is like photoluminescence or thermoluminescence in solids

---

[4] https://www.haystack.mit.edu/ast/arrays/Edges/

(Chen & McKeever 1997). Emission in the rotational lines of H_2 and HD molecules from the forming Population III objects and protogalaxies in Dark Ages have been studied by Kamaya & Silk (2002, 2003), Omukai & Kitayama (2003), Mizusawa et al. (2005), and other authors. The marginal possibility of their detection by current and future facilities and their importance have been discussed as well. The gas clouds or halos that have large peculiar velocity along the line of sight are another source of secondary anisotropy: the resonant scattering of CMB quanta by molecules in moving halos may cause increase or decrease of the brightness temperature of the radiation passing through the halo, depending on the direction of peculiar velocity relative to the observer. This was predicted by Dubrovich (1977) and the possibility of its observation was studied in Maoli et al. (1994, 1996), Dubrovich et al. (2008), Núñez-López et al. (2006), Basu (2007), Persson et al. (2010), and other papers.

The gas in the halos, which have been virialized at $10 \leqslant z \leqslant 50$, is overdensed and reheated (Novosyadlyj et al. 2018): the range of matter density is $\sim 10^{-24}$–10^{-22} g cm^{-3}, the range of gas temperature heated adiabatically is ~ 50–800 K, and that heated by shocks in processes of violent relaxation to virial temperature is $\sim 10^4$–10^5 K. Hence, the dark ages halos can be a detectable source of thermal emission in the molecular lines of the most abundant molecules, H_2 and HD. Here we estimate the brightness temperature of the molecular lowest rotational energy level emission from dark ages halos under the condition of radiative and collisional excitation.

The paper is structured as follows. In Section 2 we briefly describe the models of halos, their physical characteristics, and chemical composition. In Section 3 we describe computations of the rates of collisional excitations of the lowest five rotational levels of hydrogen molecules by atomic hydrogen and estimate the critical number density of perturbers. The methods we use to compute the populations and excitation temperatures of these levels are presented in Section 4. In Section 5 we present the results of computations of opacity, differential brightness temperatures, and differential spectral fluxes caused by thermal collisions of hydrogen molecules with hydrogen atoms. In Section 6 we compute for the same halos and lines the differential brightness temperatures and fluxes caused by the resonant scattering of the CMB radiation. Conclusions are provided in Section 7.

In the Appendix we provide a table with data for all halos analyzed in this paper, tables with coefficients of interpolations, tables with the main results, and animations showing the evolution of opacities and differential brightness temperatures for halos of different mass.

2. Models of Dark Ages Halos

We set the physical conditions and chemistry of the halos by modeling the evolution of individual spherical perturbations in the four-component universe (cold dark matter, baryon matter, dark energy, and thermal relict radiation), starting from the linear stage at the early epoch, through the quasi-linear stage, turnaround point, and collapse up to a virialized state (Novosyadlyj et al. 2016, 2018). All physical values and the chemical composition of a halo with mass $M_h = 5.3 \times 10^9 M_\odot$, which are necessary for computation of the excitations and brightness temperatures in the molecular rotational lines, are presented in Table 1. The data for halos of other masses, 6.6×10^8, 8.3×10^7, 1.0×10^7 and $1.3 \times 10^6 M_\odot$, are presented in Table 11.

All computations in the paper are performed for consistent values of the main parameters of the cosmological model, namely, the Hubble constant $H_0 = 70$ km s^{-1} Mpc^{-1}, the mean density of baryonic matter in the units of critical one $\Omega_b = 0.05$, the mean density of dark matter $\Omega_m = 0.25$, the mean density of dark energy $\Omega_{de} = 0.7$, its equation of state parameter $w = -0.9$, and the effective sound speed $c_s = 1$ (in units of speed of light). The models with dark energy with $w = $ const and cold dark matter (CDM) often are noted as wCDM. The dark matter can be also warm dark matter (WDM) with a mass of particles larger than a few keV.

We suppose that the halo is spherical and homogeneous (top-hat) with values of matter density, kinetic temperature, and the number density of species obtained from the computations of its formation. The mass of each halo M_h in the solar mass, its radius in comoving coordinates r_h (kpc), and the wavenumber k (Mpc^{-1}) of initial perturbation from which the halo is formed, are connected by relations

$$\frac{M_h}{M_\odot} = 1159 \Delta_v (1 + z_v)^3 \Omega_m h^2 r_h^3 = 4.5 \times 10^{12} \Omega_m h^2 k^{-3},$$

where z_v is the redshift of halo virialization, $\Delta_v \equiv \rho_m(z_v)/\bar{\rho}_m(z_v)$, $\Omega_m \equiv \bar{\rho}_m(0)/\rho_{cr}(0)$, $h \equiv H_0/100$ km s^{-1} Mpc^{-1}. They are presented in Tables 1 and 11. The angular sizes of the analyzed halos, θ_h, are in the range $\sim 0.\!''06$–$1.\!''25$ (last columns of Tables 1 and 11). In the computations we assume $\Delta_v = 178$.

The values of the matter density, kinetic temperature of the baryon component and radius of the halo, presented in Table 1, do not change after virialization. The number density of neutral hydrogen atoms ($n_{\text{H\,I}}$) is practically unchanged, while the number densities of molecules, protons (n_p), and electrons (n_e) are monotonically changed since molecular reactions continue. Therefore, we present their values in Tables 1 and 11 at z_v and $z = 10$, and in the computations we use the model values at any z.

3. Excitation/De-excitation Rates of H_2 and HD Rotational Levels

In this paper we analyze the possible line emission of molecules H_2 and HD caused by spontaneous transitions between the lowest rotational levels with quantum numbers $J = 0, 1, \ldots 5$ in the dark ages halos before reionization at $z \geqslant 10$. They can be excited by quanta of CMB, collisions of these molecules with atoms and molecules, and slight light backgrounds of first stars at the end of the Dark Ages. The rotational quantum numbers of allowed transitions $J_u - J_l$, Einstein coefficients A_{ul}, frequencies ν_{ul}, and energy of levels[5] E_u of molecules H_2 and HD are presented in Table 2.

The collisional excitations are crucially important since they make it possible to separate the luminous halos from the CMB background, i.e., to detect them. The bases of the theory of collisional excitation of the lowest rotational levels of molecules, which are important for observational radioastronomy, have been initiated in the papers Purcell (1952), Takayanagi & Nishimura (1960), Takayanagi (1963), Field et al. (1966), Rogers & Barrett (1968), and Goss & Field (1968). Computations of excitation/de-excitation rate of the lowest rovibrational levels of molecules H_2 by collisions with

---

[5] http://www.cv.nrao.edu/php/splat/advanced.php

Table 1
Physical Values and Chemical Composition of Halos Virialized at Different z_v

M_h ($M_\odot$)	k (Mpc^{-1})	C_k	z_v	ρ_m (g cm^{-3})	T_K (K)	$n_{\rm H\,I}$ (cm^{-3})	$n_p \approx n_e$ (10^{-6} cm^{-3})	$n_{\rm H2}$ (10^{-6} cm^{-3})	$n_{\rm HD}$ (10^{-9} cm^{-3})	r_h (kpc)	θ_h (arcsec)
5.3×10^9	5	3.0×10^{-4}	30.41	1.52×10^{-23}	402.1	1.14	106.2/3.8	14.39	2.51	1.78	1.03
		2.5×10^{-4}	25.15	8.79×10^{-24}	298.9	0.66	66.1/4.0	5.99	2.07	2.14	1.05
		2.0×10^{-4}	19.90	4.49×10^{-24}	206.3	0.34	36.7/4.0	2.15	1.51	2.68	1.09
		1.5×10^{-4}	14.65	1.89×10^{-24}	124.3	0.14	17.0/4.4	0.63	0.52	3.60	1.15
		1.0×10^{-4}	9.41	5.55×10^{-25}	59.8	0.04	5.6/5.0	0.13	0.08	5.38	1.26

Note. M is the total mass, C_k is the amplitude of initial curvature perturbation (seed of halo), z_v is the redshift of virialization, ρ_m is the matter density virialized halo, T_K is the kinetic temperature of baryonic gas, $n_{\rm H\,I}$ is the number density of neutral hydrogen atoms, n_p and n_e are the number densities of protons and electrons at $z = z_v/10$, $n_{\rm H2}$ and $n_{\rm HD}$ are the number densities of molecules H_2 and HD, r_h is the radius of the halo in comoving coordinates, and θ_h is the angular radius of the geometrically limited halo.

Table 2
The Values of Spontaneous Transitions Allowed by Quantum Selection Rules, Frequencies, and Energy for the Lowest Five Rotational Energy Levels of Hydrogen Molecules, H_2, and Hydrogen Deuteride Molecules, HD

Species	Transitions[a] J_u–J_l	A_{ul} (s^{-1})	Frequency ν_{ul} (GHz)	E_u (K)
H_2	2–0	2.94×10^{-11}	10 621	510
	3–1	4.76×10^{-10}	17 594	1 015
	4–2	2.75×10^{-9}	24 410	1 681
	5–3	9.83×10^{-9}	31 011	2 503
HD	1–0	5.32×10^{-8}	2 675	128
	2–1	5.05×10^{-7}	5 332	384
	3–2	1.80×10^{-6}	7 952	766
	4–3	4.31×10^{-6}	10 518	1 271
	5–4	8.35×10^{-6}	13 015	1 895

Note.
[a] Here and below u means upper level, and l means lower level.

hydrogen atoms have been done by Flower (1997), Flower & Roueff (1998), Wrathmall et al. (2007), Lique et al. (2012), and Lique (2015). The data by Flower (1997), Flower & Roueff (1998), and Wrathmall et al. (2007) contain the rate coefficients of collision transitions between rovibrational levels with $\Delta J = \pm 2, \pm 4, \ldots$ up to 26th level for both spin isomers: the ortho-hydrogen and para-hydrogen molecules. They are available at the Ro-Vibrational Collisional Excitation Database of the VAMDC consortium[6], which also contains the analytical fits of their dependences on temperature, which are accurate for the temperature range 100–6000 K. We use these fits for the de-excitation rate coefficients of para-/ortho-H_2 by atomic hydrogen for $T_K \geqslant 100$ K; for the lower temperatures we use the extrapolation by second-order polynomial on the base of the nearest three data points. The coefficients for fits and extrapolations of collisional de-excitation κ_{ul} of the lowest rotational levels of molecules para-H_2 ($J = 0, 2, 4$) and ortho-H_2 ($J = 1, 3, 5$) used here are presented in the Appendix in Tables 12 and 13 accordingly. The collisional excitation rate coefficients κ_{lu} are computed using the well known relation $\kappa_{lu} = \kappa_{ul} g_u/g_l / \exp(h\nu_{ul}/kT_K)$. The dependences of the coefficients of the collisional rate excitations/de-excitations of three lowest levels of para-/ortho-H_2 molecules by atomic hydrogen on temperature are shown in the left panel of Figure 1. We take into account the transition ortho $\leftrightarrows$ para using the ratio $n_{\rm ortho}/n_{\rm para}$ computed by Flower & Pineau des Forêts (2000) for

the temperature range 1–10^4 K. We also estimate the impact of new collisional coefficients by Lique (2015) on the excitation temperatures of rotational transitions of ortho-/para-H_2 and brightness temperatures in the most intensive lines.

Computations of excitation/de-excitation rate coefficients of the lowest rovibrational levels of hydrogen deuteride molecules, HD, by collisions with hydrogen atoms have been done by Flower & Roueff (1999) and Roueff & Flower (1999). The complete results for the most transitions with $\Delta J = 1, 2, \ldots$ for levels with $J = 0, \ldots 9$ and $v = 0, 1, 2$ are available at the database of the VAMDC consortium for the temperature range 100–2080 K with step $\Delta T_K = 20$ K. They are approximated by cubic polynoms in the log–log scale that is shown in the right panel of Figure 1. The best-fit coefficients are presented in Table 14 in the Appendix of the on-line version. For temperatures lower than 100 K we use the extrapolated values issued by this fit.

The rates of collisional excitation/de-excitation of lower (l)/upper (u) levels of molecules H_2 and HD (noted as X) are computed as follows:

$$C_{ul}^X = \kappa_{ul}^X n_{\rm H}, \qquad C_{lu}^X = \kappa_{lu}^X n_{\rm H}.$$

In Figure 2 we show the inverse rate collisional and radiative excitations, C_{lu}^{-1} and $(B_{lu} U_{\nu_{ul}})^{-1}$, as well as de-excitations, C_{ul}^{-1} and $(B_{ul} U_{\nu_{ul}})^{-1}$, in the halos virialized at different z for comparison with the actual age of the universe, t_U, and the character times of number density changes of molecules, which are estimated as follows $(|d \ln n_X/dt|)^{-1} = (|(z + 1)H(z)d \ln n_X/dz|)^{-1}$. Here and below $U_{\nu_{ul}}$ notes the energy density of CMB radiation at the frequency of transition between levels u and l. One can see that in the dark ages halos for molecules H_2 the rates of collisional excitation/de-excitation by atomic hydrogen are comparable with the rates of radiative excitation/de-excitation by CMB quanta. At the high redshifts they are close to the value of the rate of spontaneous transition A_{ul} to the base level (Table 2). For molecules HD in the conditions of dark ages halos the rates of collisional excitation/de-excitation are a few orders lower than the radiative ones and the rates of spontaneous transitions (Table 2).

The values presented in Figure 2 also show that for halos formed at $z > 30$ ($T_K > 400$ K, $n_{\rm H} > 10^6$ m^{-3}) the character times of collisional and radiation excitations/de-excitations of levels 2–5 of H_2 are lower than the age of the universe and the character time of the number density change of molecular hydrogen. This means that the population of the rotational levels of molecular hydrogen can be estimated using a condition of quasi-stationarity. Later, at $z \leqslant 30$, when the adiabatic temperature of virialized halos is <400 K, the character times of collisional and radiation excitations of levels 2–5 are comparable and higher than the age
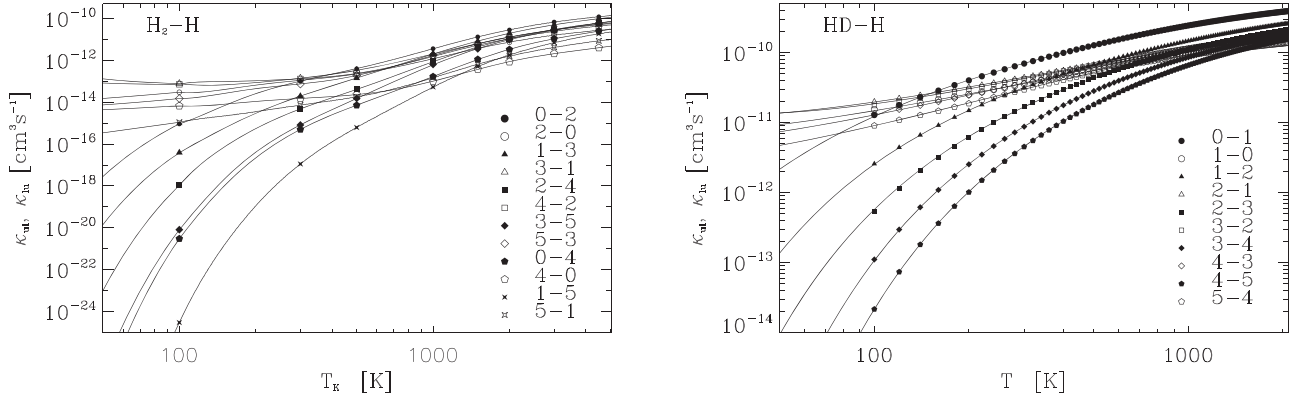
Figure 1. Rate coefficients for collisional excitation (κ_{lu}, filled symbols) and de-excitation (κ_{ul}, open symbols) of molecules H_2 and HD by H.
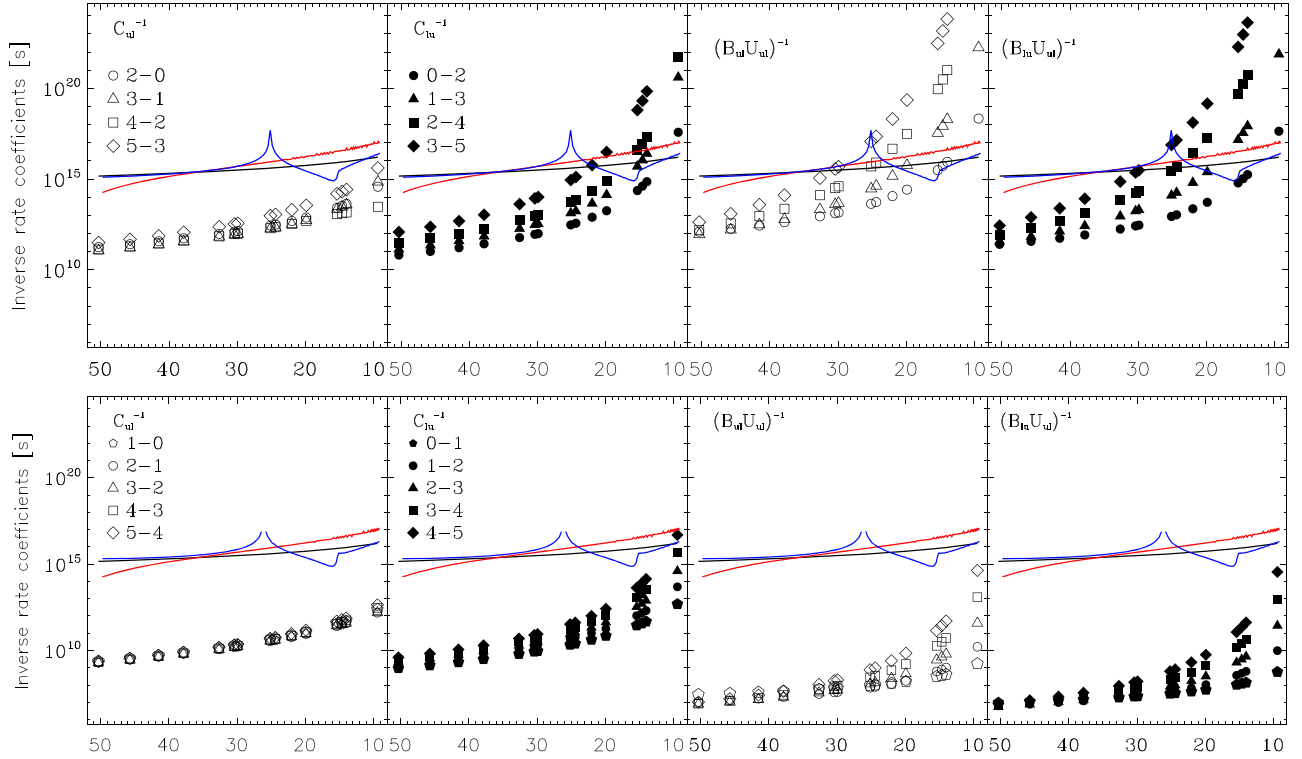

Figure 2. Inverse rate coefficients C_{ul}^{-1}, C_{lu}^{-1}, $(B_{ul}U_{\nu_{ul}})^{-1}$, and $(B_{lu}U_{\nu_{ul}})^{-1}$ for molecules H_2 (top panel) and HD (bottom panel) in halos virialized at different z. The black solid line shows the age of the universe corresponding to z, the red solid line shows the character times of the number density changes of molecules H_2/HD in a halo virialized at $z \approx 50$ and a blue line at $z \approx 15$.

of the universe, hence the condition of quasi-stationarity for populations of the rotational levels there cannot be used. For molecules HD this condition can practically always be used for dark ages halos.

The data for rates of spontaneous transitions allowed by quantum selection rules and rates of their collisional de-excitations illustrate the emission properties of halos in general. For any transition between levels u and l, there is a critical number density of perturbers, n_H^{cr}, at which the radiating molecule suffers collisions at the rate $C_{ul} = A_{ul}$. It means that for $n_H \gg n_H^{cr}$ collisional de-excitations are dominated over spontaneous radiation transitions. In this case the thermal emission in the line vanishes.

The critical densities of atomic hydrogen for each level discussed here can be estimated as $n_H^{cr} = A_{ul}/\kappa_{ul}$. The results of computations are presented in Figure 3. The critical densities for the lowest rotational levels of molecular hydrogen, H_2, and hydrogen deuteride, HD, are essentially larger than the density

of the atomic hydrogen in the halos. This means that the thermal emission in these lines is expected. The problem is to extract it from the CMB background.

4. Populations and Excitation Temperatures of Rotational Levels with $J = 0-5$

Let's consider the six-levels system and all collision and radiative transition permitted by the quantum selection rules. Since the conditions of quasi-stationarity in the halos virialized at $z < 30$ are not satisfied for all levels of the H_2 molecule kinetic equations for transitions between levels must be solved. The selection rules for the H_2 molecule (electric quadrupole transitions) permit $\Delta J = \pm 2$ for radiative transitions, for the HD molecule (electric dipole transitions) they permit $\Delta J = \pm 1$, so the kinetic equations for populations of the rotational levels for these molecules are different.
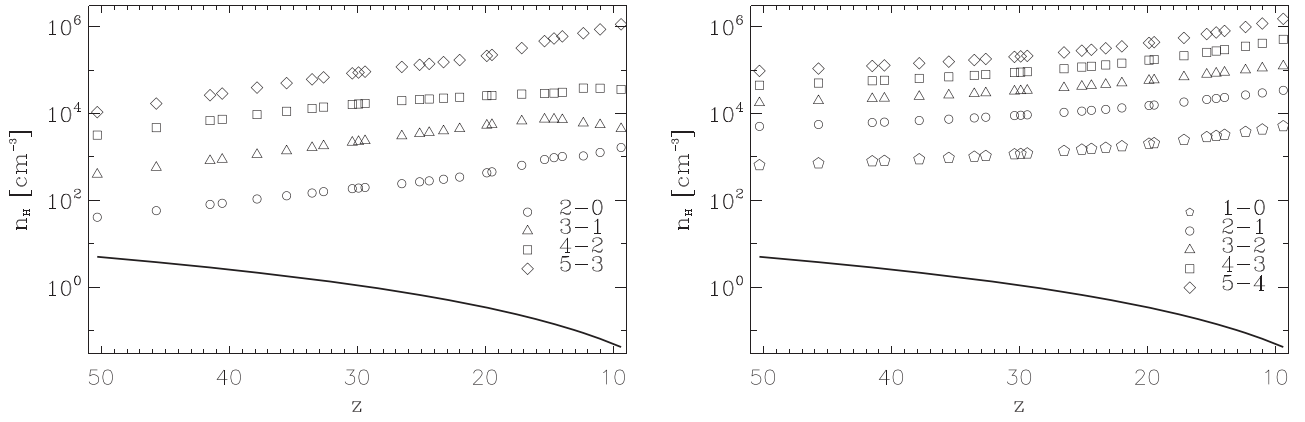
Figure 3. Critical number density for the lowest energy levels of molecular hydrogen (left panel) and hydrogen deuteride (right panel) in the dark ages halos virialized at different redshifts. The solid line shows the real values of number density of molecular hydrogen in the halos virialized at z.

In the general case before and after virialization the kinetic equations for populations of the rotational levels of H_2 and HD are as follows:

H_2:

$$(1 + z)H\frac{dX_j}{dz} = X_j(R_{j\,j+2} + C_{j\,j+4})$$
$$- X_{j+2}R_{j+2\,j} - X_{j+4}C_{j+4\,j}, \quad j = 0, 1$$
$$(1 + z)H\frac{dX_j}{dz} = X_j(R_{j\,j-2} + R_{j\,j+2})$$
$$- X_{j-2}R_{j-2\,j} - X_{j+2}R_{j+2\,j}, \quad j = 2, 3$$
$$(1 + z)H\frac{dX_j}{dz} = X_j(R_{j\,j-2} + C_{j\,j-4})$$
$$- X_{j-2}R_{j-2\,j} - X_{j-4}C_{j-4\,j}, \quad j = 4, 5$$

$$(1)$$

HD:

$$(1 + z)H\frac{dY_0}{dz} = Y_0\left(R_{01} + \sum_{i=2}^{5}C_{0i}\right) - Y_1R_{10} - \sum_{i=2}^{5}Y_iC_{i0},$$
$$(1 + z)H\frac{dY_j}{dz} = Y_j\left(R_{j\,j-1} + R_{j\,j+1} + \sum_{i\neq j,j\pm1}^{5}C_{ji}\right)$$
$$- Y_{j-1}R_{j-1\,j} - Y_{j+1}R_{j+1\,j} - \sum_{i\neq j,j\pm1}^{5}Y_iC_{ji}, \quad j = 2, 3, 4$$
$$(1 + z)H\frac{dY_5}{dz} = Y_5\left(R_{54} + \sum_{i=0}^{3}C_{5i}\right) - Y_4R_{45} - \sum_{i=0}^{3}Y_iC_{i5},$$

$$(2)$$

where $X_j \equiv n_j/n_{H_2}$ and $Y_j \equiv n_j/n_{HD}$ are fractions of molecular hydrogen and hydrogen deuteride correspondingly in the state with rotational quantum number $J = j$, $R_{ul} = A_{ul} + B_{ul}U_{\nu_{ul}} + C_{ul}$, $R_{lu} = B_{lu}U_{\nu_{ul}} + C_{lu}$. One equation from system (1) for H_2 can be substituted by the simple equation

$$\frac{n_1^{H_2} + n_3^{H_2} + n_5^{H_2}}{n_0^{H_2} + n_2^{H_2} + n_4^{H_2}} = \frac{n_{ortho}}{n_{para}},$$

$$(3)$$

and one equation from system (2) for HD can be substituted by

$$n_0^{HD} + n_1^{HD} + n_2^{HD} + n_3^{HD} + n_4^{HD} + n_5^{HD} = n_{HD} \quad (4)$$

after their differentiation with respect to redshift.

We integrate Equations (1)–(2) with the code $ddriv1$[7] together with equations of evolution of temperature and density of all components as well as with kinetic equations of formation/destruction of molecules in the halo (Novosyadlyj et al. 2018). We set the initial conditions for Equations (1)–(2) assuming that at $z \geqslant 200$ the quasi-stationary condition is satisfied and we solve the system of algebraic equations for H_2 and HD separately. In this way we obtain the evolution of populations of the rotational levels, opacities, and the line intensities at all stages of the formation and existence of dark ages halos.

Dark ages halos after virialization have unchanged density, temperature, and chemical composition, hence the conditions of stationarity of populations of energy levels are satisfied for them. In this case the left parts of Equations (1)–(2) are zero,

$$\frac{dX_j}{dz} = 0, \quad \frac{dY_j}{dz} = 0,$$

and we have two systems of algebraic Equations ((1) and (2)) that can be solved by standard methods if their last equations, for example, are substituted by Equations (3)–(4) correspondingly. We use for that the subroutine dgesv.f from lapack library.

When the populations of the rotational levels are computed, we can calculate the excitation temperatures for $l - u$ levels:

$$T_{ex} = \frac{h\nu_{ul}}{k_B}\left[\ln\frac{g_u n_l}{g_l n_u}\right]^{-1}.$$

They are presented for $l - u$ levels of molecules H_2 and HD in Tables 3 and 4 accordingly for the dark ages halos with mass $M_h = 5.3 \times 10^9 \, M_\odot$ and different initial amplitudes of matter density perturbations, which are virialized at $z = 30.41$, 25.15, 19.90, 14.65, and 9.41. The kinetic temperatures of gas in halos and CMB temperature are presented for comparison. For values of $T_{ex} - T_R > 0$, the halos are warmer spots in the CMB. Note that these values are essentially larger for H_2 molecules than for HD molecules. This is the case because the hydrogen deuteride molecule is asymmetrical, has a nonzero electric dipole moment and more effectively interacts with radiation. The data in Table 2 and in Figure 2 support this explanation.

The excitation temperatures of the lowest rotational levels of molecular hydrogen are sensitive to the ratio of n_{ortho}/n_{para} and

---

7 http://www.netlib.org/slatec/src/ddriv1.f

Table 3
The Excitation Temperatures for the Lowest Rotational Levels of H_2 Molecules in the Halos Formed at the Redshifts $z = 30-10$

z	T_K (K)	T_R (K)	T_{ex} (K)			
			0–2	1–3	2–4	3–5
30.41	402.1	85.6	93.7	93.3	113.4	145.7
25.15	298.9	71.3	76.1	77.5	102.9	130.3
19.90	206.3	57.0	59.7	62.7	89.5	108.6
14.65	124.3	42.7	43.8	48.1	69.9	79.4
9.41	59.8	28.4	28.8	32.9	43.7	44.6

Table 4
The Excitation Temperatures for the Lowest Rotational Levels of HD Molecules in the Halos Formed at the Redshifts $z = 30-10$

z	T_K (K)	T_R (K)	T_{ex} (K)			
			0–1	1–2	2–3	3–4
30.41	402.1	85.61	85.71	85.64	85.63	85.63
25.15	298.9	71.27	71.32	71.29	71.28	71.28
19.90	206.3	56.96	56.98	56.97	56.97	56.97
14.65	124.3	42.65	42.66	42.66	42.66	42.66
9.41	59.8	28.37	28.37	28.37	28.37	28.37

Table 5
Opacity of Halos with $M_h = 5.3 \times 10^9 \, M_\odot$ Virialized at Different Redshifts, z_v, in the Lowest Rotational Levels of Molecular Hydrogen, H_2

z_v	τ_{ul}			
	2–0	3–1	4–2	5–3
30.41	8.67×10^{-9}	4.24×10^{-8}	5.23×10^{-10}	2.94×10^{-11}
25.15	4.99×10^{-9}	2.48×10^{-8}	8.55×10^{-11}	2.74×10^{-12}
19.90	2.67×10^{-9}	1.35×10^{-8}	7.26×10^{-12}	1.13×10^{-13}
14.65	1.43×10^{-9}	6.64×10^{-9}	1.76×10^{-13}	9.45×10^{-16}
9.41	9.40×10^{-10}	2.60×10^{-9}	2.72×10^{-16}	1.09×10^{-19}

Table 6
The Opacity of Halos with $M_h = 5.3 \times 10^9 \, M_\odot$ Virialized at Different Redshifts, z_v, in the Lowest Rotational Levels of Hydrogen Deuteride Molecules, HD

z_v	τ_{ul}			
	1–0	2–1	3–2	4–3
30.41	2.25×10^{-7}	1.23×10^{-7}	9.69×10^{-9}	1.51×10^{-10}
25.15	3.17×10^{-7}	1.22×10^{-7}	5.18×10^{-9}	3.28×10^{-11}
19.90	4.28×10^{-7}	9.93×10^{-8}	1.69×10^{-9}	2.78×10^{-12}
14.65	3.12×10^{-7}	3.23×10^{-8}	1.21×10^{-10}	2.09×10^{-14}
9.41	1.25×10^{-7}	2.74×10^{-9}	4.98×10^{-13}	9.58×10^{-19}

values of rate coefficients of their collisional excitation/de-excitation by atomic hydrogen. We recompute the transitions ortho $\leftrightarrows$ para and populations of the rotational levels using the rate coefficients revised by Lique (2015). It resulted in some differences with the data of Flower & Pineau des Forêts (2000): in the temperature range 1000–10 K, the ratio n_{ortho}/n_{para} changes in the range 1–1.3 instead of 2.8–0.3. The excitation temperatures, however, do not change so radically: differences do not exceed 4% for the first excited levels of para- and ortho-H_2 with $J = 2$ and $J = 3$ accordingly. But the populations of these levels changed more significantly: in the temperature range of ~400–60 K the population of the first excited level of para-H_2 increases by 1.7–2.2 times, while the population of the first excited level of ortho-H_2 decreases by 1.6–3.2 times.

5. Opacity and Brightness Temperature of Dark Ages Halos in Rotational Lines of Molecules H_2 and HD

The opacity at the frequency of the $u - l$ transition is calculated in the rest frame of the halo as

$$\tau_{ul} = \int_0^{r_h} \alpha_{\nu_{ul}}(r) dr,$$

where $\alpha_{\nu_{ul}}$ is the absorption coefficient per unit of length in frequency ν_{ul}, and r_h is the radius of the halo.

The absorption coefficient per unit of length in frequency ν_{ul} is as follows (formulas (2.69) and (2.154) in Lang 1974):

$$\alpha_{\nu_{ul}} = \frac{c^2}{8\pi \nu_{ul}^2} \frac{n_l}{\Delta \nu_L} \frac{g_u}{g_l} \left[1 - \exp\left(-\frac{h\nu_{ul}}{k_B T_{ex}}\right) \right] A_{ul}, \quad (5)$$

where n_l is the number density of molecules in the lower level l, k_B is Boltzmann constant, A_{ul} is the spontaneous transition probability (Einstein coefficient), T_{ex} is the excitation temperature for the $u - l$ transition, and $\Delta \nu_L$ is the width of the line at half-maximum. The last value in the case of the virialized halo can be treated like the case of a turnaround

halo (Maoli et al. 1996):

$$\frac{\Delta \nu_L}{\nu} = \frac{2}{c} \sqrt{\frac{2 \ln 2 \, k_B T_K}{m}} = 7.16 \times 10^{-7} \sqrt{\frac{T_K}{m_A}}, \quad (6)$$

where T_K is the kinetic temperature (adiabatic or virial) of gas in a halo, and m and m_A are the atomic mass and atomic number of a molecule, respectively. In the visible center of the spherical homogeneous top-hat halo the optical depth in rotational line ν_{ul} is as follows

$$\tau_{ul} = 1.55 \times 10^{50} n_l \frac{g_u}{g_l} \frac{A_{ul}}{\nu_{ul}^3} \sqrt{\frac{m_A}{T_k}} \left[1 - \exp\left(-\frac{h\nu_{ul}}{k_B T_{ex}}\right) \right] r_h, \quad (7)$$

where r_h is its radius in units of megaparsecs (the rest values must be in the CGS system).

The results of computations of τ_{ul} for the lowest rotational levels of molecules para-/ortho-H_2 and HD are presented in Tables 5 and 6 accordingly. The opacities in the frequency ν_{31} of the ortho-H_2 molecule are larger than those in the frequency ν_{20} of the para-H_2 molecule because $n_{ortho}/n_{para} \approx 3$ (Flower & Pineau des Forêts 2000). They decrease with decreasing z_v because the number density of molecules decreases (Table 1), as well as the populations of non-base levels of both molecules via decreasing of excitation temperatures (Tables 3 and 4). The opacity related to the base level of the HD molecule is not monotonic function of z_v (2nd column of Table 6), since its population ($n_{J=0}/n_{HD}$) fast increases with decreasing excitation temperature.

We note also, that the opacities of the dark ages halos in the rotational lines of the HD molecule are higher than those in the lines of the H_2 molecule in spite of the $n_{HD}/n_{H_2} \sim 10^{-4}$. This has a simple explanation: the factor A_{ul}/ν_{ul}^2 in (5) is essentially larger for HD than for H_2.

We also have analyzed the evolution of opacities of single halos during its formation. The results for the brightest lines of H_2 and HD molecules for halos with mass $M_h = 5.3 \times 10^9 \, M_\odot$ and different initial amplitudes of density perturbation are presented in the left panels of Figures 4 and 5 accordingly. The
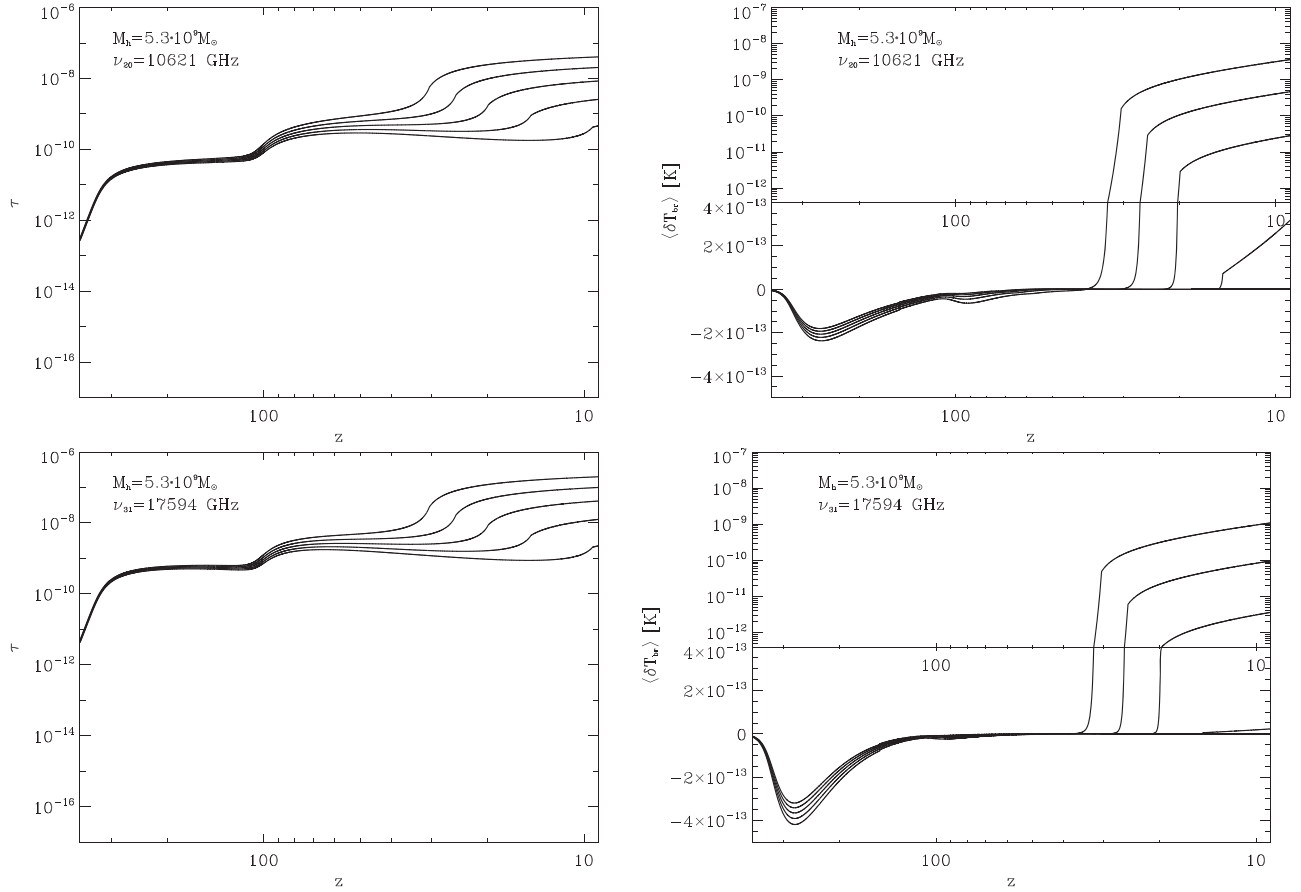
Figure 4. Evolution of opacity (left column) and brightness temperature (right column) in the lines of transitions $J = 2 \rightarrow 0$ (top row) and $J = 3 \rightarrow 1$ (bottom row) of the H_2 molecule for halos with mass $M_h = 5.3 \times 10^9 \, M_\odot$. Each line corresponds to halos with different initial amplitudes of curvature perturbation: $C_k = 3 \times 10^{-4}$, 2.5×10^{-4}, 2×10^{-4}, 1.5×10^{-4}, 1×10^{-4} (from top to bottom on right side side of each panel.

same results for other lines and other halos are presented in the animate Figures 8 and 9 in Appendix of the on-line version. One can see that halos that formed earlier have larger opacities at lower redshifts compared to halos that formed at the same redshifts, since they are denser.

The differential brightness temperature for thermal emission is obtained from the radiative transfer equation and is as follows

$$\delta T^b_{ul} = \frac{h\nu_{\rm obs}}{k_{\rm B}} \left[\frac{1}{e^{\frac{h\nu_{ul}}{k_{\rm B}T_{\rm ex}}} - 1} - \frac{1}{e^{\frac{h\nu_{ul}}{k_{\rm B}T_R}} - 1} \right] (1 - e^{-\tau_{ul}}),$$

where T_b is the Rayleigh–Jeans brightness temperature, $T_{\rm ex}$ is the excitation temperature of the $u - l$ transition and T_R is the temperature of the background radiation. The dark ages halos are optically thin in the molecular lines, so $(1 - e^{-\tau_{ul}}) \approx \tau_{ul}$, and the expression for the brightness temperature of thermal emission of dark ages halos becomes

$$\delta T^b_{ul} = \frac{7.44 \times 10^{39} n_u A_{ul}}{(1+z)\nu^2_{ul}} \sqrt{\frac{m_A}{T_K}} \left[\frac{e^{\frac{h\nu_{ul}}{k_{\rm B}T_R}} - e^{\frac{h\nu_{ul}}{k_{\rm B}T_{\rm ex}}}}{e^{\frac{h\nu_{ul}}{k_{\rm B}T_R}} - 1} \right] \frac{r_h}{1\,{\rm Mpc}}, \quad (8)$$

where n_u is in units of cm^{-3}. Since the observable differential brightness temperature is not homogeneous on the surface of the halo we can average it like

$$\langle \delta T_{\rm br} \rangle = 2 \int_0^1 \delta T_{\rm br}(x) x \, dx,$$

where $x = \theta/\theta_h$. In our case the integral has an exact analytical presentation that for small values of τ_{ul} gives factor $2/3$:

$$\langle \delta T^b_{ul} \rangle = \frac{2}{3} \delta T^b_{ul}. \quad (9)$$

Expression (8) provides the possibility to understand when a thermal emission signal from dark ages halos can be sighted in the CMB. This requires additional perturbers in order for $T_{\rm ex} > T_R$. If $T_{\rm ex} \rightarrow T_R$ then $\delta T^b_{ul} \rightarrow 0$. The halos should be dense and extended to have large opacities. The emitting molecules must be abundant and have a large value of the ratio of Einstein coefficients to square frequency for excited levels. The maximal value of differential brightness temperature is expected in the case when $T_{\rm ex} \gg h\nu_{ul}/k_{\rm B}$ and the value in brackets in (8) is close to 1.

We use the data from Tables 1, 11, and 2 to compute the differential brightness temperatures in the lowest rotational frequencies of the H_2 and HD molecules for halos formed at $z = 10$–50. The results for halos with $M_h = 5.3 \times 10^9 \, M_\odot$ are presented in Tables 7 and 8 for the H_2 and HD molecules, respectively. First, note that the thermal emission of dark ages halos in the low rotational level of molecules H_2 and HD exists but the values of differential brightness temperatures are too low to be detected by current instrumentation. The values are larger for halos virialized earlier and vanishes for halos virialized later.
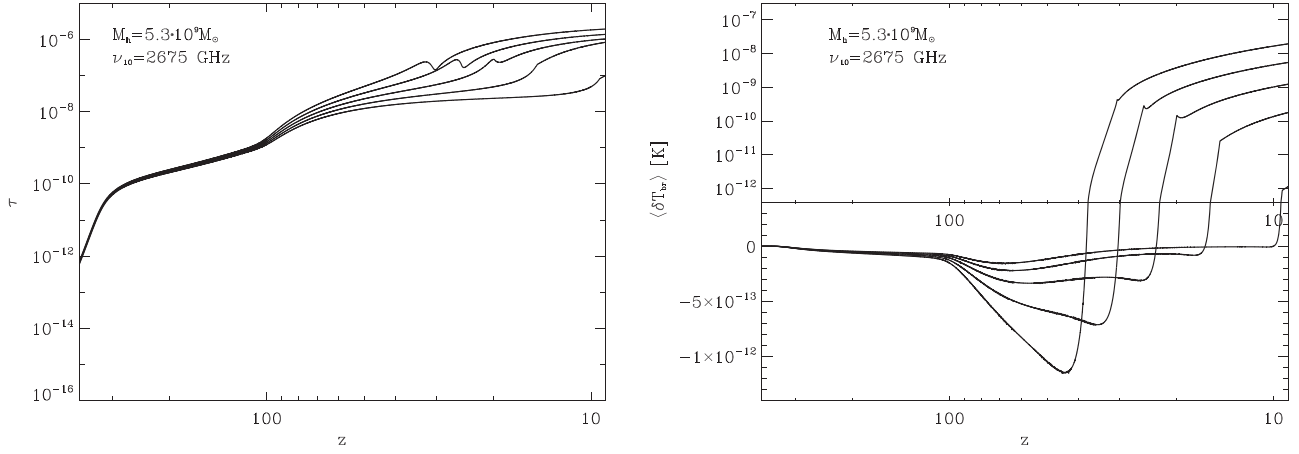
Figure 5. Evolution of opacity (left column) and brightness temperature (bright column) in the lines of transitions $J = 1 \rightarrow 0$ of the HD molecule for halos with mass $M_h = 5.3 \times 10^9 \, M_\odot$. Each line corresponds to halos with different initial amplitudes of curvature perturbation, as in the previous figure.

Table 7
Thermal Emission: The Differential Brightness Temperatures of Halos with $M_h = 5.3 \times 10^9 \, M_\odot$ Virialized at Different Redshifts, z_v, in the Lowest Rotational Levels of Molecular Hydrogen, H_2

z_v	$\langle \delta T_{ul}^b \rangle$ (K)			
	2–0	3–1	4–2	5–3
30.41	1.64×10^{-10}	4.92×10^{-11}	4.08×10^{-13}	3.40×10^{-14}
25.15	2.92×10^{-11}	6.13×10^{-12}	2.87×10^{-14}	1.12×10^{-15}
19.90	2.87×10^{-12}	3.82×10^{-13}	5.61×10^{-16}	6.03×10^{-18}
14.65	7.57×10^{-14}	5.13×10^{-15}	4.63×10^{-19}	4.33×10^{-22}
9.41	1.55×10^{-16}	9.80×10^{-19}	4.53×10^{-26}	3.39×10^{-32}

Table 8
Thermal Emission: The Differential Brightness Temperatures of Halos with $M_h = 5.3 \times 10^9 \, M_\odot$ Virialized at Different Redshifts, z_v, in the Lowest Rotational Levels of Hydrogen Deuteride Molecules, HD

z_v	$\langle \delta T_{ul}^b \rangle$ (K)			
	1–0	2–1	3–2	4–3
30.41	4.28×10^{-10}	5.32×10^{-11}	2.02×10^{-12}	3.68×10^{-14}
25.15	2.84×10^{-10}	2.29×10^{-11}	4.66×10^{-13}	4.50×10^{-15}
19.90	1.45×10^{-10}	6.08×10^{-12}	4.94×10^{-14}	2.00×10^{-16}
14.65	2.59×10^{-11}	3.44×10^{-13}	5.98×10^{-16}	6.11×10^{-19}
9.41	9.01×10^{-13}	9.67×10^{-16}	6.33×10^{-20}	3.60×10^{-24}

We also have analyzed the evolution of differential brightness temperature in the rotational lines of H_2 and HD of single halos during its formation. The results are shown for the lowest transitions $(J = 2 \rightarrow 0 / J = 3 \rightarrow 1$ for para-/ortho-H_2 and $J = 1 \rightarrow 0$ HD molecules) in the right panels of Figures 4 and 5 for halos with mass $M_h = 5.3 \times 10^9 \, M_\odot$. The results for other transitions and halos of other masses are presented in the animated versions of Figures 8 and 9 in the Appendix. These figures are a combination of logarithmic and normal scales since before the turnaround of halos and since the beginning of the collapse; the differential brightness temperatures have been negative since $T_{ex} < T_R$ because the adiabatic temperature of gas is lower than the CMB temperature, $T_K < T_R$. In the case of the HD molecule we see the deep lowering of the brightness temperature for transition $J = 1 \rightarrow 0$, a slight decrease for transition $J = 2 \rightarrow 1$ and its absence for transitions between upper levels before the appearance of emission. Their amplitudes, however, are too small to discuss the possibility of their observations.

Another measure of the halo signal extracted from the cosmic background radiation is the differential energy flux per unit frequency (Iliev et al. 2002):

$$\delta F_{ul} = \frac{2\pi}{c} \left(\frac{\nu_{ul}}{1+z} \right)^2 k_B \langle \delta T_{ul}^b \rangle \theta_h^2$$
$$= \frac{2.27}{(1+z)^2} \left(\frac{\nu_{ul}}{1 \, \text{GHz}} \right)^2 \left(\frac{\langle \delta T_{ul}^b \rangle}{1 \, \text{K}} \right) \left(\frac{\theta_h}{1''} \right)^2 \, \mu\text{Jy}. \quad (10)$$

For the values of differential brightness temperatures presented in Tables 7 and 8 the values of differential energy flux, $\delta F_{ul} \leqslant 10^{-5} \, \mu$Jy. In Tables 15 and 16 we present them for the rest halos

and the two lowest transitions of the H_2 and HD molecules. We obtain the maximal values of differential energy fluxes for a halo of maximal mass $M_h = 5.3 \times 10^9 \, M_\odot$, which virialized earliest ($z_v = 30.41$). For example, in the frequency 338 GHz (transition $J = 2 \rightarrow 0$ of para-H_2 molecule) it is $\sim 4 \times 10^{-5} \, \mu$Jy. The maximal flux in the frequency 85 GHz ($J = 1 \rightarrow 0$) of the HD molecule is estimated as $\sim 7 \times 10^{-6} \, \mu$Jy. Both values are essentially lower than the sensitivity of current radio telescopes.

The small values of expected molecular hydrogen emission from dark ages halos could be caused by low values of adiabatic temperature. However, the virialization temperatures of halos can be larger than adiabatic temperatures caused by smooth homogeneous collapse (Barkana & Loeb 2001; Bromm & Yoshida 2011; Novosyadlyj et al. 2018). Local inhomogeneities, shock waves, fragmentation, and other nonlinear phenomena will enhance the kinetic temperature of gas in halos. We estimate the differential brightness temperature of dark ages halos in the rotational lines of hydrogen molecules for higher kinetic temperatures of gas in the virialized halos, which had the same history before. We suppose that halos after virialization reach some temperatures $T_{K(\text{vir})} > T_{K(\text{ad})}$ independent of the redshift of virialization. The results for $T_{K(\text{vir})} = 1000, 2000, 5000$ K are presented in Figure 6. Increasing the kinetic temperature of gas in the virialized halos leads to an increase of their differential brightness temperature in the rotational lines of molecular hydrogen. We see that for para/ortho-hydrogen molecules the effect of temperature is larger than that for hydrogen deuteride ones, and the baseline of ortho-H_2 is more intensive than para-H_2. The values of the differential brightness temperatures of hot halos

Figure 7. The rms peculiar velocity averaged in the top-hat sphere with radius R at different redshifts in the wCDM model with post-Planck cosmological parameters (Planck Collaboration et al. 2018a).

Table 9
Resonant Scattering: The Differential Brightness Temperatures of Halos with $M_h = 5.3 \times 10^9 M_\odot$ Virialized at Different Redshifts, z_v, in the Lowest Rotational Levels of Molecular Hydrogen, H_2

z_v	$\langle\delta T_{ul}^b\rangle$ (K)			
	2–0	3–1	4–2	5–3
30.41	1.53×10^{-11}	4.11×10^{-12}	2.13×10^{-15}	4.78×10^{-18}
25.15	3.49×10^{-12}	4.34×10^{-13}	2.92×10^{-17}	1.77×10^{-20}
19.90	4.31×10^{-13}	1.68×10^{-14}	5.57×10^{-20}	5.39×10^{-24}
14.65	1.75×10^{-14}	8.77×10^{-17}	2.09×10^{-24}	1.08×10^{-29}
9.41	5.15×10^{-17}	2.95×10^{-21}	5.83×10^{-33}	5.36×10^{-41}

Table 10
Resonant Scattering: The Differential Brightness Temperatures of Halos with $M_h = 5.3 \times 10^9 M_\odot$ Virialized at Different Redshifts, z_v, in the Lowest Rotational Levels of Hydrogen Deuteride Molecules, HD

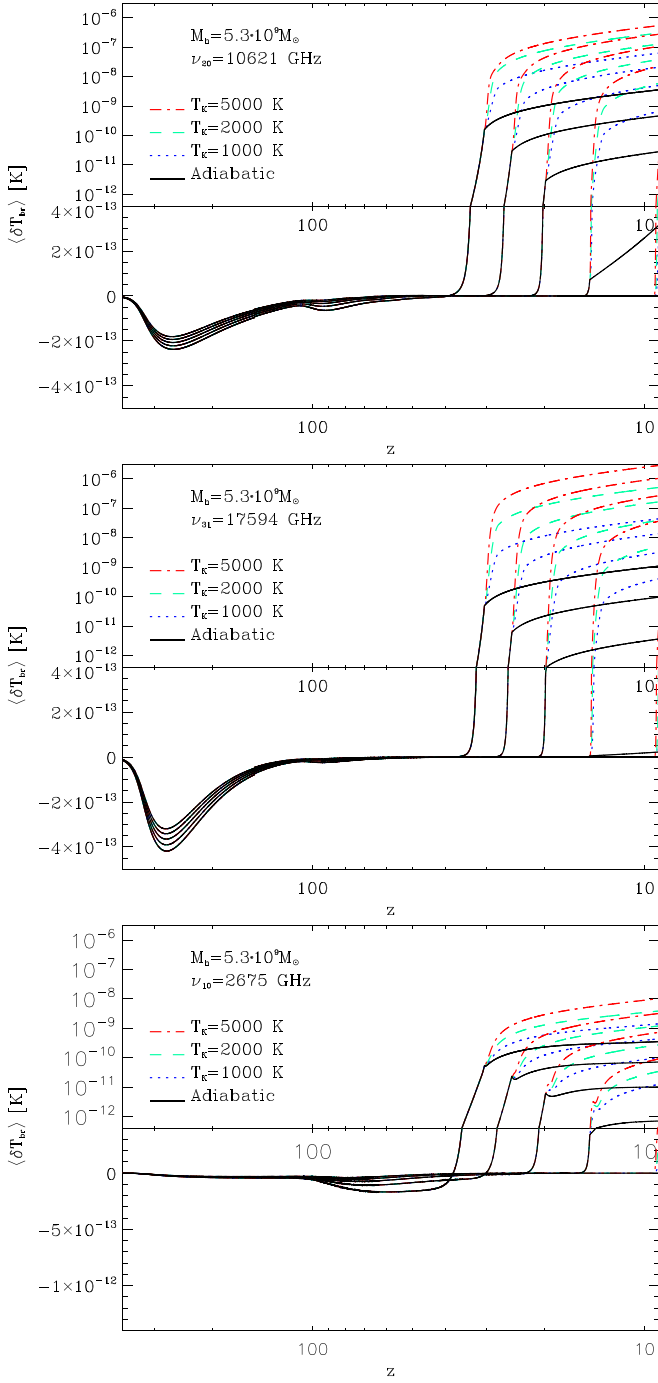| z_v	$\langle\delta T_{ul}^b\rangle$ (K)			
	1–0	2–1	3–2	4–3
30.41	3.57×10^{-9}	1.17×10^{-9}	4.37×10^{-11}	2.77×10^{-13}
25.15	4.24×10^{-9}	7.98×10^{-10}	1.23×10^{-11}	2.41×10^{-14}
19.90	4.42×10^{-9}	3.56×10^{-10}	1.45×10^{-12}	4.80×10^{-16}
14.65	2.06×10^{-9}	3.86×10^{-11}	1.68×10^{-14}	2.84×10^{-19}
9.41	3.05×10^{-10}	2.90×10^{-13}	1.40×10^{-18}	6.13×10^{-26}

Figure 6. Evolution of brightness temperature in the lines of transitions $J = 2 \rightarrow 0$ and $J = 3 \rightarrow 1$ of the H_2 molecule and $J = 1 \rightarrow 0$ of the HD molecule for halos with mass $M_h = 5.3 \times 10^9 M_\odot$. Each line corresponds to the halo with different initial amplitude of curvature perturbation, following previous figures and different final temperatures.

$(T_{K \,(\text{vir})} \gtrsim 2000$ K) are comparable with the sensitivity of the *Planck* observatory (Planck Collaboration et al. 2018b) and the expected sensitivity of the SKA radio telescope that is being built, $\langle\delta T_{ul}^b\rangle \sim 10^{-6}$ K. Both, unfortunately, are far from the angular resolution, which is necessary to detect individual halos analyzed here.

It is interesting to compare our results with estimations of H_2 and HD emission in the same lines from the primordial object, either Population III galaxies or primordial clouds, which have been computed and discussed by Kamaya & Silk (2002, 2003),
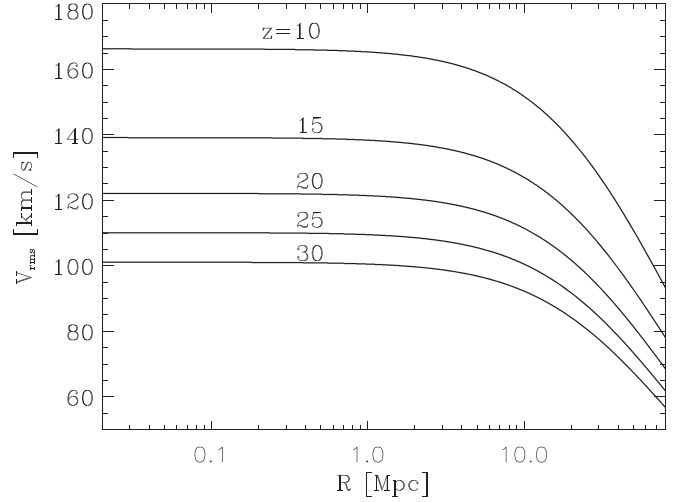
Omukai & Kitayama (2003), and Mizusawa et al. (2005). The expected emission flux from the molecular cloud cores at the redshift of $z \sim 20$ in the $J = 2 \rightarrow 0$ line of H_2 is $\sim 2 \times 10^{-7}$ Jy, and that in the $J = 4 \rightarrow 3$ line of HD is $\sim 8 \times 10^{-9}$ Jy (Kamaya & Silk 2003). The differential spectral fluxes δF in these lines at $z \sim 24$ from the smallest halos analyzed here are 3×10^{-15} and 3×10^{-19} Jy accordingly. Since the differential brightness temperature δT_{br} in those lines are 1.5×10^{-12} K and 1.9×10^{-16} K respectively, and $\delta F \propto \delta T_{\text{br}}$, and $F \propto T_{\text{br}}$ with the same coefficient of proportion, the spectral fluxes in these lines are $\sim 5 \times 10^{-3}$ Jy. Omukai & Kitayama (2003) have estimated the energy fluxes in the rotational lines of H_2 molecule from forming galaxies at $z = 20$: 8×10^{-27} erg cm^{-2} s $(J = 2 \rightarrow 0)$ and 5.6×10^{-26} erg cm^{-2} s $(J = 3 \rightarrow 1)$ for galaxies with $M = 10^7 M_\odot$, and 9×10^{-24} erg cm^{-2} s $(J = 2 \rightarrow 0)$ and

7.7×10^{-23} erg cm^{-2} s ($J = 3 \rightarrow 1$) for galaxies with $M = 10^9 M_\odot$. According to our results (Table 15 in the Appendix), the fluxes in these lines are as follows: 8×10^{-22}erg cm^{-2} s ($J = 2 \rightarrow 0$) and 3.6×10^{-21} erg cm^{-2} s ($J = 3 \rightarrow 1$) for galaxies with $M = 10^7 M_\odot$, and 7×10^{-20} erg cm^{-2} s ($J = 2 \rightarrow 0$) and 3.2×10^{-19} erg cm^{-2} s ($J = 3 \rightarrow 1$) for galaxies with $M = 5.3 \times 10^9 M_\odot$. So, fluxes in lower rotational lines of hydrogen and hydrogen deuteride molecules from dark ages halos analyzed here are ~4 order higher than the fluxes in the same lines from other primordial objects. Such a large difference is caused mainly by the difference in structural models of sources and the mechanisms of excitation/de-excitation of the rotational levels. In our case the excitation by CMB is dominant, but in foregoing studies the thermal luminescence has been analyzed.

We also estimate how the predictions of opacities of halos and brightness temperatures in the lines of transitions between rotational levels of ortho-/para-H$_2$ change with collision rate coefficients revised by Lique (2015). In the line of transition $J = 0 \rightarrow 2$ (para-H$_2$) the opacities increase by 1.2–1.8 times for the halos virialized at $z = 30$–10, while in the line of transition $J = 1 \rightarrow 3$ (ortho-H$_2$) the opacities decrease by 1.1–1.7 times. These differences, as well as the change in the populations of the levels and excitation temperatures, lead to changes in the differential brightness temperature. In the halos with kinetic temperature $\gtrsim$170 K the differential brightness temperature in the baseline of para-H$_2$ ($J = 2 \rightarrow 0$) increases by 1.4–1.7 times, and for colder halos it increases by 3.5–5.4 times. In contrast, the baseline of ortho-H$_2$ ($J = 3 \rightarrow 1$), decreases by 1.7–2.6 times for warmer halos and decreases ~3.5 times for colder ones. Hence, the main conclusion of this reanalysis is that revised collisional excitation/de-excitation coefficients do not change the main results and conclusions.

6. Resonant Scattering

The resonant scattering of CMB quanta in the rotational lines of molecules in the dark ages halo that has optical depth τ_{ul} and peculiar velocity v_p, leads to differential brightness temperature (Maoli et al. 1996; Persson et al. 2010)

$$\delta T_{ul}^b = \frac{h^2 \nu_{ul}^2}{k_B^2 T_R} \frac{\tau_{ul}}{(1 - e^{-\frac{h\nu_{ul}}{k_B T_R}})^2} \frac{v_p}{c} \cos\theta, \qquad (11)$$

where θ is the angle between the vector of peculiar velocity and the line of sight of the terrestrial observer. The rms value of the peculiar velocity averaged over the spherical region with radius R can be estimated if the power spectrum $P(k; z)$ of initial density perturbations is known:

$$\langle v_p^2 \rangle = \frac{H^2(z)}{2\pi^2 (1 + z)^2} \int_0^\infty P(k; z) W^2(kR) dk, \qquad (12)$$

where $W(x) \equiv 3(\sin x - x\cos x)/x^3$ is the top-hat sphere in Fourier space. We present the $V_{rms} \equiv \langle v_p^2 \rangle^{1/2}$ as a function of smoothing scale R for the power spectrum of the wCDM model with post-Planck cosmological parameters (Planck Collaboration et al. 2018a, 2018b) in Figure 7. For the power spectrum $P(k; z) \equiv A_s(z) k^{n_s} T^2(k; z)$ we have normalized, by computation of $\sigma_8 = 0.806$, the current epoch using the fitting formula for the transfer function $T(k; z)$, proposed by Eisenstein & Hu (1998). We rescaled the amplitude $A_s(z)$ for different redshifts using the square of the growth function $D(z)$ by Carroll et al. (1992).

We compute the absolute values of differential brightness temperature δT_{ul}^b and spectral flux δF_{ul} caused by resonant scattering in the same rotational lines of para-H$_2$, ortho-H$_2$, and HD molecules for the same halos. The results are presented in Tables 9–10 and 15–16 in the Appendix. They show that expected amplitudes of intensities of emission/absorption in the rotational lines of both isomers of molecular hydrogen caused by resonant scattering are by order and lower than those caused by thermal collisions with adiabatically warmed gas in the dark ages halos. And in contrast, the amplitudes of halo intensities in the rotational lines of the HD molecule caused by resonant scattering are systematically higher than thermal emission intensities. The effect is more noticeable at small redshifts ($z \sim 10$–15), where the signal is much weaker.

Signals caused by resonant scattering increase with the opacity of halos such as thermal halos, but decrease when radiation and gas temperatures increase. Hence, the warm halos ($T_K \sim 400$ K) are brighter in the HD rotational lines ($\nu_{obs} \sim 85$ GHz) caused by resonant scattering, while the hot halos ($T_K \sim 2000$ K) are brighter in the line of ortho-H$_2$ ($\nu_{obs} \sim 338$ GHz) caused by thermal collisions with hydrogen atoms.

The estimations of the differential brightness temperature caused by the resonant scattering in the first rotational levels of the hydrogen deuteride molecule in the dark ages halos presented here are comparable with the values obtained by Núñez-López et al. (2006). They computed the secondary anisotropy of CMB caused by resonant scattering in HD lines of top-hat halos of the wide mass range 10^2–$10^{12} M_\odot$ at the stages of their turnaround and after virialization. They have constrained themselves by analyzing the halos that formed from the overdensity with the initial amplitude of relative density perturbations $\delta\rho/\bar\rho \sim 3\sigma$ and 6σ, where σ is the value of rms density perturbations at the corresponding scale. We study the halos with initial amplitudes of curvature perturbations $C_k = 1.5$–3×10^{-4} (seed of halos) that are in the same range of peak heights (see Section 2.1 in Novosyadlyj et al. 2018). The opacities in the rotational lines $J = 1$–0, 2–1, and 3–2 in the left panel of Figures 5 and 9 for halos with a mass of $5.3 \times 10^9 M_\odot$ and corresponding initial amplitudes are comparable with opacities computed by Núñez-López et al. (2006) (Figures 2 and 3) for the halos at their turnaround points (in our figures they are at $z = 46$, 38, 30, 22, and 15 for lines, from top to bottom). The secondary anisotropy of CMB $\Delta T/\bar T$ caused by resonant scattering in halos at the turnaround point computed by Núñez-López et al. (2006) is in the range $\sim 10^{-10}$–10^{-12} for the first rotational transition of the HD molecule. Our computations give the values $\sim 3 \times 10^{-12}$–2×10^{-14} for halos of mass $5.3 \times 10^9 M_\odot$ and initial amplitudes from the range 3σ-6σ. They will be larger for halos with larger masses. For the virialized halos Núñez-López et al. (2006) obtained $\sim 2 \times 10^{-5}$–10^{-8}. Our estimations for hot halos fall within this range of values (Figure 6).

Since the peculiar velocities of different halos have a random amplitude and direction, the superposition of these effects gives the rms total amplitude of the differential brightness temperature $\langle \delta T_{ul}^b \rangle = [\langle (\delta T_{ul}^{b(th)})^2 \rangle + \langle (\delta T_{ul}^{b(rs)})^2 \rangle]^{1/2}$, where the angle parentheses represent ensemble averaging.

7. Conclusions

We have analyzed the emission of dark ages halos in the lines of transitions between the lowest rotational levels of hydrogen molecules, para-H$_2$, ortho-H$_2$, and HD. It was assumed that halos are homogeneous top-hat spheres formed from the cosmological density perturbations in the four-component universe with

post-Planck cosmological parameters. We have considered the excitation/de-excitation of the lowest five rotational levels of hydrogen molecules by CMB radiation and thermal collisions with atomic hydrogen. The kinetic equations for populations of the energy levels have been solved in two independent ways, which give the close final values of differential brightness temperatures of virialized halos caused by thermal collisions. The first one consists of the integration of systems of differential kinetic equations for populations of the levels, together with systems of differential equations of evolution of cosmological perturbations and kinetic equations of formation/destruction of the first molecules. The results of numeric integration, presented in Figures 4–6 and 8–9 in the Appendix, show the dependence of opacities and differential brightness temperatures on the redshift from the early stage of halo formation to the virialized final stage. The second part of the analysis consists of the solution of the system of algebraic equations for the populations of the lowest rotational levels of H_2 and HD molecules in the virialized halos. These solutions provide the possibility to compute the excitation temperatures of levels, the differential brightness temperatures, and fluxes in the lines of transitions between them, which are presented in Tables 3–8 and 15–16 in the Appendix. Both methods give practically the same values for the populations of levels, opacities, differential brightness temperatures, and spectral fluxes for virialized halos. We also compute the differential brightness temperatures and spectral fluxes in the same lines caused by resonant scattering of CMB radiation for the halos with an rms value of peculiar velocity at different redshifts. The results are presented in Tables 9–10 and in the last two columns of Tables 15–16 in the Appendix.

Our main conclusions are as follows. (1) The dark ages halos are a source of emission in the lines of transitions between the lowest rotational levels of hydrogen molecules excited by CMB radiation and collisions with atoms of neutral hydrogen. (2) The amplitudes of differential brightness temperatures caused by thermal collisions with H are systematically larger in the rotational lines of ortho-H_2 and para-H_2 molecules than in the lines of HD ones. The maximal values are reached for the earliest warm small halos ($z_v \sim 50$, $T_K \sim 800$ K, $M_h \sim 10^6\ M_\odot$),

but they do not exceed nanokelvin at $\nu_{\mathrm{obs}} \sim 200$–300 GHz. (3) The amplitudes of differential brightness temperatures in the lowest rotational lines of HD molecules caused by resonant scattering are systematically higher than those caused by thermal collisions with H for halos with peculiar velocity equal to rms one followed from the power spectrum of cosmological perturbations and directed to/from the terrestrial observer. The maximal values that are reached are about few nanokelvins at $\nu_{\mathrm{obs}} \sim 85$–170 GHz for the massive warm halos ($z_v \sim 20$, $T_K \sim 200$ K, $M_h \sim 5 \times 10^9\ M_\odot$). (4) If the dark ages halos are hot after virialization ($T_K \sim 2000$–5000) then the differential brightness temperatures caused by thermal collisions increase by a few orders, reaching values of a few microkelvins, which may be achievable for the next-generation telescopes.

Appendix
Supplementary Material

Animated Figures 8 and 9 illustrate the evolution of the opacities and brightness temperatures in the rotational lines of hydrogen and hydrogen deuteride molecules for halos with different masses (frames) virialized at different redshifts (lines). Table 11 is continuation of Table 1 for halos of lower masses. The best-fit coefficients of analytical approximations for collisional deactivation of rotational levels of molecules, which are used in this paper, are presented in Tables 12–14. The continuation of Tables 5–8, containing the main results, are Tables 15 and 16 for the halos of lower masses.

Figure 8. First still image from an animation of the evolution of opacity (left column) and brightness temperature (bright column) in the lines of transitions $J = 2 \rightarrow J = 0$ (upper row), $J = 3 \rightarrow J = 1$ (middle row), and $J = 4 \rightarrow J = 2$ (bottom row) of molecular hydrogen. Each line corresponds to a halo with different initial amplitudes of curvature perturbation: $C_k = 3 \times 10^{-4}, 2.5 \times 10^{-4}, 2 \times 10^{-4}, 1.5 \times 10^{-4}, 1 \times 10^{-4}$ (from top to bottom on the right side of each panel. There are 5 frames in the 10 second animation. Each frame appears for 2 seconds and corresponds to halo mass in sequence $M_h = 1.3 \times 10^6 \, M_\odot$, $M_h = 1.0 \times 10^7 \, M_\odot$, $M_h = 8.3 \times 10^7 \, M_\odot$, $M_h = 6.6 \times 10^8 \, M_\odot$, and $M_h = 5.3 \times 10^9 \, M_\odot$, respectively.

(An animation of this figure is available.)

Figure 9. First still image from an animation of the evolution of opacity (left column) and brightness temperature (bright column) in the lines of transitions $J = 1 \rightarrow J = 0$ (upper row), $J = 2 \rightarrow J = 1$ (middle row), and $J = 3 \rightarrow J = 2$ (bottom row) of HD molecules. Each line corresponds to a halo with different initial amplitudes of curvature perturbation: $C_k = 3 \times 10^{-4}, 2.5 \times 10^{-4}, 2 \times 10^{-4}, 1.5 \times 10^{-4}, 1 \times 10^{-4}$ (from top to bottom on the right side of each panel. There are 5 frames in the 10 second animation. Each frame appears for 2 seconds and corresponds to halo mass in sequence $M_h = 1.3 \times 10^6 \, M_\odot$, $M_h = 1.0 \times 10^7 \, M_\odot$, $M_h = 8.3 \times 10^7 \, M_\odot$, $M_h = 6.6 \times 10^8 \, M_\odot$, and $M_h = 5.3 \times 10^9 \, M_\odot$, respectively.

(An animation of this figure is available.)

Table 11
Physical Values and Chemical Composition of Halos Virialized at Different z_v

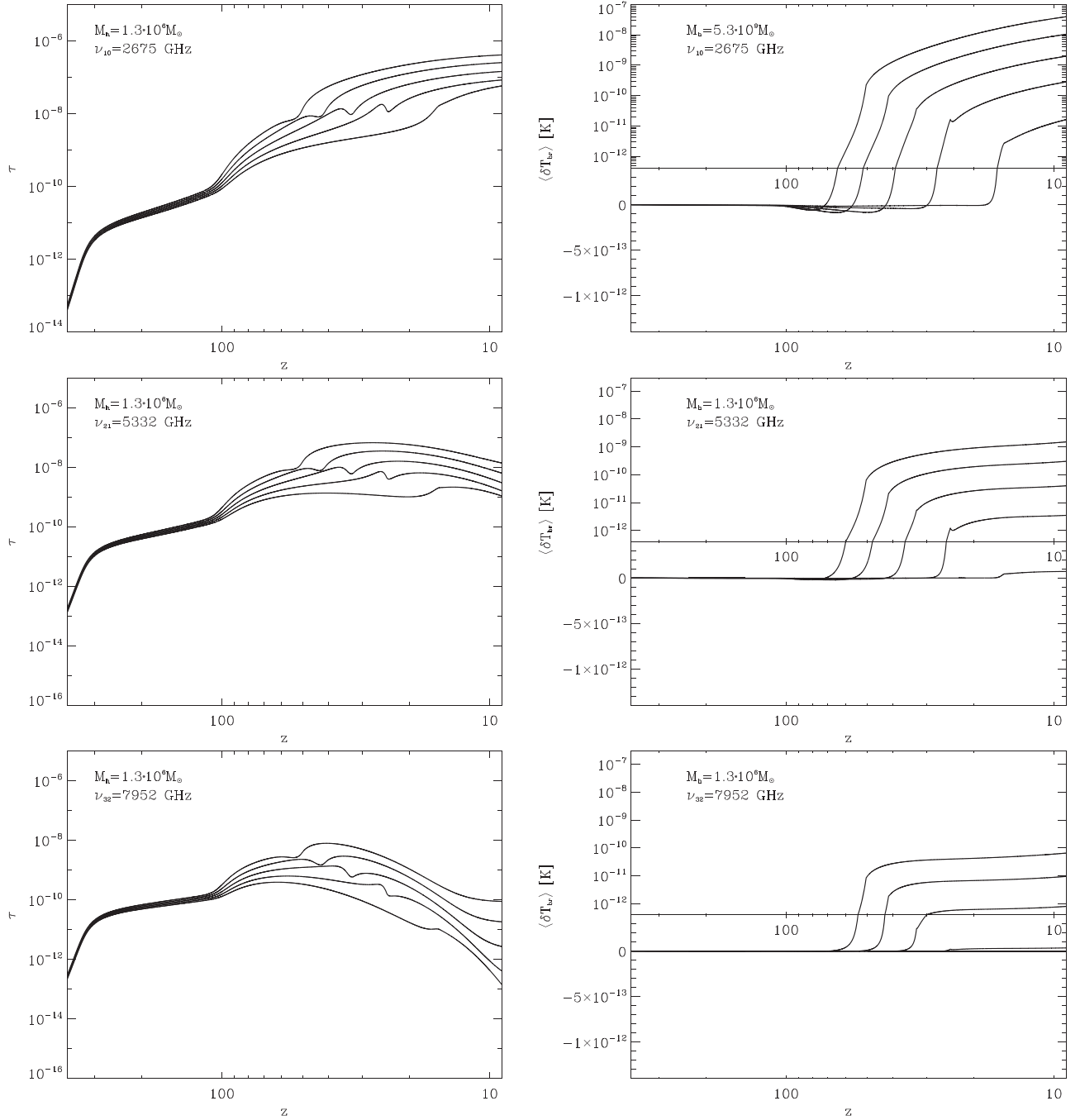| M_h $(M_\odot)$	k (Mpc^{-1})	C_k	z_v	ρ_m $(\mathrm{g\,cm}^{-3})$	T_K (K)	$n_{\mathrm{H\,I}}$ (cm^{-3})	$n_p \approx n_e$ $(10^{-6}\,\mathrm{cm}^{-3})$	$n_{\mathrm{H_2}}$ $(10^{-6}\,\mathrm{cm}^{-3})$	n_{HD} $(10^{-9}\,\mathrm{cm}^{-3})$	r_h (kpc)	θ_h ('')
6.6×10^8	10	3.0×10^{-4}	35.54	2.40×10^{-23}	508.9	1.80	156.3/3.7	30.32	3.83	0.77	0.50
		2.5×10^{-4}	29.41	1.38×10^{-23}	382.8	1.04	97.4/3.8	12.41	2.36	0.92	0.52
		2.0×10^{-4}	23.28	7.05×10^{-24}	266.3	0.53	54.2/3.9	4.29	1.94	1.15	0.53
		1.5×10^{-4}	17.17	2.95×10^{-24}	162.1	0.22	25.1/4.2	1.18	0.98	1.54	0.56
		1.0×10^{-4}	11.05	8.60×10^{-25}	78.2	0.06	8.3/4.7	0.23	0.16	2.32	0.61
8.3×10^7	20	3.0×10^{-4}	40.57	3.54×10^{-23}	619.2	2.65	214.5/3.7	58.54	6.24	0.34	0.25
		2.5×10^{-4}	33.55	2.03×10^{-23}	468.4	1.52	133.5/3.7	23.71	3.25	0.40	0.25
		2.0×10^{-4}	26.54	1.03×10^{-23}	325.5	0.77	74.0/3.8	7.96	2.10	0.51	0.26
		1.5×10^{-4}	19.50	4.24×10^{-24}	199.6	0.32	33.8/4.0	2.08	1.46	0.68	0.27
		1.0×10^{-4}	12.36	1.17×10^{-24}	94.0	0.09	10.4/4.5	0.36	0.30	1.05	0.30
1×10^7	40	3.0×10^{-4}	45.72	5.01×10^{-23}	730.3	3.76	287.2/3.6	103.8	9.94	0.15	0.12
		2.5×10^{-4}	37.85	2.88×10^{-23}	556.0	2.16	179.7/3.7	40.91	4.78	0.18	0.13
		2.0×10^{-4}	29.92	1.46×10^{-23}	392.9	1.09	99.7/3.8	13.97	2.45	0.23	0.13
		1.5×10^{-4}	22.02	6.00×10^{-24}	242.8	0.45	45.7/3.9	3.53	1.80	0.30	0.13
		1.0×10^{-4}	14.00	1.66×10^{-24}	115.2	0.13	14.1/4.3	0.58	0.50	0.47	0.14
1.3×10^6	80	3.0×10^{-4}	50.33	6.66×10^{-23}	834.0	5.00	355.3/3.6	172.5	15.40	0.068	0.061
		2.5×10^{-4}	41.52	3.78×10^{-23}	636.5	2.84	218.8/3.7	69.78	7.28	0.082	0.062
		2.0×10^{-4}	32.65	1.87×10^{-23}	446.8	1.41	117.7/3.7	23.12	3.25	0.10	0.064
		1.5×10^{-4}	24.40	8.07×10^{-24}	286.1	0.61	58.6/3.9	5.68	1.94	0.14	0.066
		1.0×10^{-4}	15.38	2.16×10^{-24}	134.4	0.16	17.1/4.2	0.89	0.78	0.21	0.071

Note. M is the total mass, C_k is the amplitude of initial curvature perturbation (seed of halo), z_v is the redshift of virialization, ρ_m is the matter density virialized halo, T_K is the kinetic temperature of baryonic gas, $n_{\mathrm{H\,I}}$ is the number density of neutral hydrogen atoms, n_p and n_e are the number densities of protons and electrons at $z = z_v/10$, $n_{\mathrm{H_2}}$ and n_{HD} are the number densities of molecules $\mathrm{H_2}$ and HD, r_h is the radius of the halo in comoving coordinates, and θ_h is the angular radius of the geometrically limited halo.

Table 12
The Best-fit Coefficients of Analytical Approximation of the Dependences of the Collisional Deactivation Rate Coefficients on the Kinetic Temperature, T_K, by Formula $\lg\kappa_{ul}(T_K) = \sum_{k=0}^{N-1} a_k^{(ul)}(\lg T_K/\epsilon^{(ul)})^k + a_N^{(ul)}(1/(T_K/\epsilon^{(ul)} + \epsilon^{(ul)}) - 1)$ for the $\mathrm{H_2}$ Molecule (Solid Lines in the Left Panel of Figure 1)

u	l	ϵ	a_0	a_1	$a2$	a_3	a_4	a_5	a_6	a_7	a_8
2	0	6.0	−8259.36044	1846.12284	−4713.51503	3907.15150	−1672.56520	4015.80145	−51.6262545	2.78079268	−9095.89801
3	1	15.0	1402.43596	−58.1010752	74.2671058	18.8773370	−36.2141786	12.2012441	−1.32412404	0.00000000	1484.70110
4	2	15.0	11533.9595	2070.41178	−4153.50389	5002.05894	−3171.93991	1091.80410	−195.457394	14.3495151	12713.2249
5	3	13.0	5064.45306	73.5896891	−266.094034	722.660337	−590.299001	223.156022	−41.0457115	2.98641025	5439.61121
4	0	24.0	6887.91049	−219.803978	673.503903	−912.827587	802.461038	−395.623746	98.4201969	−9.67987032	7148.50271
5	1	61.0	76184.3307	76.4032424	−87.2258173	387.822432	−476.720251	397.196415	−157.426338	22.3504536	77451.1227

Note. It is valid in the temperature range $100 \leqslant T_K \leqslant 6000$ K. The coefficients are taken from the VAMDC database; the misprints in the formula have been fixed.

Table 13
The Best-fit Coefficients of Analytical Approximation of the Dependences of the Collisional Deactivation Rate Coefficients on the Kinetic Temperature, T_K, by Quadratic Parabola for $\mathrm{H_2}$ Molecule for Temperature Range 50–500 K (Solid Lines in the Left Panel of Figure 1)

u	l	a_0	a_1	$a2$
2	0	−14.653	0.066487	0.24931
3	1	−6.0491	−6.8089	1.6397
4	2	−9.5234	−3.7050	0.94767
5	3	−13.942	−1.0658	0.56254
4	0	−14.910	0.072763	0.14760
5	1	−18.092	0.1.4405	0.063031

Table 14
The Best-fit Coefficients of Analytical Approximation of the Dependences of the Collisional Deactivation Rate Coefficients for the HD Molecule on the Kinetic Temperature, T_K, by Polynom of 3D Order, $\lg\kappa_{ul}(T_K) = a_{ul} + b_{ul}\lg T_K + c_{ul}(\lg T_K)^2 + d_{ul}(\lg T_K)^3$ (Solid Lines in the Right Panel of Figure 1)

u	l	a	b	c	d
1	0	−16.026	−2.2319	1.2578	−0.17135
2	0	−12.813	−8.2155	3.6827	−0.46921
3	0	−6.1385	−16.448	6.3996	−0.74128
4	0	8.5527	−32.399	11.634	−1.2838
5	0	2.6510	−27.177	9.7365	−1.0395
2	1	−15.293	−2.7751	1.3979	−0.18162
3	1	−12.970	−7.7509	3.4431	−0.43110
4	1	−5.8105	−16.797	6.5236	−0.75144
5	1	−2.9747	−21.584	8.2829	−0.93604
3	2	−13.998	−4.3688	2.0205	−0.25961
4	2	−13.766	−6.9609	3.1745	−0.39987
5	2	−9.2775	−13.887	5.7245	−0.67937
4	3	−16.229	−2.2922	1.3529	−0.18594
5	3	−14.639	−6.3194	3.0045	−0.38352
5	4	−16.554	−2.3252	1.4452	−0.20237

Table 15
Optical Depths, Brightness Temperatures, and Spectral Fluxes in the Two Lowest Rotational Lines of Molecule H$_2$ in the Dark Ages Halos of Different Masses, M_h, Virialized at Different Redshifts, z_v

M_h ($M_\odot$)	z_v	ν_{obs} (GHz)	$\Delta\nu_{obs}$ (kHz)	τ_ν 10^{-9}	$\delta T_{bb}^{(th)}$ (10^{-12} K)	$\delta F^{(th)}$ (10^{-12} Jy)	$\delta T_{bb}^{(rs)}$ (10^{-12} K)	$\delta F^{(rs)}$ (10^{-12} Jy)
1.29×10^6	50.33	207	3.02	1.88	799.0	0.288	16.9	0.006
		343	4.99	13.1	657.0	0.650	28.1	0.028
	41.52	250	3.18	1.39	175.0	0.095	7.55	0.004
		414	5.27	7.44	91.1	0.136	6.05	0.009
	32.65	316	3.37	0.77	22.0	0.020	1.82	0.002
		523	5.58	3.76	7.49	0.019	0.63	0.002
	24.40	418	3.57	0.31	1.51	0.003	0.18	0.0003
		693	5.91	1.55	0.30	0.001	0.02	0.00009
	15.39	648	3.79	0.11	0.01	0.00005	0.002	0.00001
		1070	6.28	0.54	0.0008	0.00001	0.00002	0.0000002
1.04×10^7	45.72	227	3.10	3.16	732.0	1.300	22.4	0.040
		377	5.14	18.7	468.0	2.280	25.4	0.124
	37.85	273	3.25	2.03	141.0	0.380	8.29	0.022
		453	5.39	10.3	61.9	0.458	4.82	0.036
	29.92	343	3.44	1.08	18.6	0.083	1.78	0.008
		569	5.69	5.29	5.45	0.066	0.45	0.005
	22.02	461	3.63	0.46	1.09	0.009	0.15	0.001
		764	6.01	2.31	0.18	0.004	0.01	0.00023
	14.00	708	3.83	0.18	0.006	0.0001	0.001	0.00003
		1170	6.35	0.82	0.0004	0.00002	0.000005	0.0000003
8.28×10^7	40.57	255	3.21	4.91	545.0	4.990	24.9	0.229
		423	5.31	25.9	273.0	6.870	18.4	0.464
	33.55	307	3.36	2.98	103.0	1.420	7.88	0.109
		509	5.56	14.6	36.8	1.400	3.02	0.115
	26.54	386	3.51	1.52	12.5	0.288	1.41	0.033
		639	5.82	7.48	2.91	0.184	0.22	0.014
	19.50	518	3.69	0.67	0.61	0.028	0.093	0.004
		858	6.12	3.38	0.078	0.010	0.003	0.0004
	12.36	795	3.89	0.32	0.0029	0.0004	0.0006	0.00008
		1320	6.44	1.24	0.0001	0.00003	0.0000007	0.0000002
6.63×10^8	35.54	291	3.31	6.82	330.0	16.1	22.4	1.09
		481	5.48	33.9	131.0	17.5	10.5	1.40
	29.41	349	3.45	3.96	61.5	4.53	6.04	0.445
		579	5.71	19.4	17.5	3.530	1.42	0.288
	23.28	437	3.60	2.03	7.27	0.893	0.91	0.112
		725	5.97	10.2	1.32	0.445	0.080	0.027
	17.17	585	3.76	0.96	0.27	0.065	0.050	0.012
		968	6.22	4.78	0.027	0.018	0.0008	0.00052

Table 15
(Continued)

M_h ($M_\odot$)	z_v	ν_{obs} (GHz)	$\Delta\nu_{obs}$ (kHz)	τ_ν 10^{-9}	$\delta T_{br}^{(th)}$ (10^{-12} K)	$\delta F^{(th)}$ (10^{-12} Jy)	$\delta T_{br}^{(rs)}$ (10^{-12} K)	$\delta F^{(rs)}$ (10^{-12} Jy)
	11.05	881	3.93	0.52	0.0011	0.0007	0.0003	0.00017
		1460	6.52	1.84	0.00002	0.00004	0.0000001	0.0000002
5.30×10^9	30.41	338	3.42	8.67	164.0	44.9	15.3	4.20
		560	5.67	42.4	49.2	37.0	4.11	3.09
	25.15	406	3.54	4.99	29.2	12.1	3.49	1.45
		673	5.87	24.8	6.13	6.98	0.43	0.494
	19.90	508	3.68	2.67	2.87	2.00	0.43	0.299
		842	6.10	13.5	0.38	0.729	0.017	0.032
	14.65	679	3.82	1.43	0.076	0.104	0.018	0.024
		1120	6.32	6.64	0.0051	0.019	0.00009	0.0003
	9.41	1020	3.98	0.94	0.00016	0.0006	0.00005	0.0002
		1690	6.60	2.60	0.000001	0.00001	0.000000003	0.00000003

Note. The values with (th) are related to the thermal emission, and the values with (rs) are related to the resonant scattering.

Table 16
Optical Depths, Brightness Temperatures and Spectral Fluxes in the Two Lowest Rotational Lines of Molecule HD in the Dark Ages Halos of Different Masses, M_h, Virialized at Different Redshifts, z_v

M_h ($M_\odot$)	z_v	ν_{obs} (GHz)	$\Delta\nu_{obs}$ (kHz)	τ_ν 10^{-9}	$\delta T_{br}^{(th)}$ (10^{-12} K)	$\delta F^{(th)}$ (10^{-12} Jy)	$\delta T_{br}^{(rs)}$ (10^{-12} K)	$\delta F^{(rs)}$ (10^{-12} Jy)
1.29×10^6	50.33	52.1	0.62	19.0	230.0	0.005	435.0	0.010
		104	1.23	21.4	65.4	0.006	401.0	0.036
	41.52	62.9	0.65	16.3	99.2	0.003	328.0	0.011
		125	1.30	14.4	21.5	0.003	217.0	0.030
	32.65	79.5	0.69	14.8	37.0	0.002	250.0	0.015
		158	1.38	9.13	5.30	0.001	98.2	0.023
	24.40	105	0.73	20.0	16.0	0.002	260.0	0.029
		210	1.46	7.25	1.20	0.0005	44.3	0.019
	15.39	163	0.78	25.9	2.69	0.0008	186.0	0.057
		325	1.55	3.09	0.044	0.00005	4.53	0.006
1.04×10^7	45.72	57.3	0.64	33.1	285.0	0.032	713.0	0.08
		114	1.27	33.2	71.4	0.032	561.0	0.25
	37.85	68.9	0.67	28.4	121.0	0.021	537.0	0.92
		137	1.33	22.0	22.7	0.015	295.0	0.20
	29.92	86.5	0.71	28.7	51.6	0.015	451.0	0.13
		172	1.41	15.3	6.20	0.007	141.0	0.16
	22.02	116	0.74	49.0	25.6	0.014	570.0	0.31
		232	1.48	14.3	1.45	0.032	67.9	0.15
	14.00	178	0.79	41.6	2.75	0.041	253.0	0.38
		355	1.57	3.75	0.03	0.0002	3.68	0.022
8.28×10^7	40.57	64.3	0.66	59.7	337.0	0.196	1190.0	0.69
		128	1.31	51.0	70.7	0.163	749.0	1.73
	33.55	77.4	0.69	54.8	153.0	0.134	944.0	0.83
		154	1.37	35.2	23.1	0.081	396.0	1.38
	26.54	97.1	0.72	69.1	77.0	0.113	973.0	1.42
		194	1.44	29.5	7.08	0.041	217.0	1.26
	19.50	130	0.76	109.0	33.9	0.097	1100.0	3.17
		260	1.51	24.1	1.33	0.015	81.3	0.93
	12.36	200	0.80	63.8	2.24	0.018	304.0	2.43
		399	1.59	3.86	0.013	0.0004	2.08	0.66
6.63×10^8	35.54	73.2	0.68	109.0	376.0	1.160	1960.0	6.08
		146	1.35	76.7	63.1	0.777	940.0	11.6
	29.41	88.0	0.71	116.0	195.0	0.913	1800.0	8.41
		175	1.41	60.0	22.7	0.421	539.0	10.0
	23.28	110	0.74	182.0	120.0	0.939	2250.0	17.5
		220	1.47	59.8	7.98	0.247	327.0	10.1
	17.17	147	0.77	201.0	35.4	0.541	1700.0	26.0
		293	1.54	32.3	0.90	0.054	71.6	4.35
	11.05	222	0.81	88.5	1.68	0.069	328.0	13.5
		442	1.61	3.62	0.0053	0.0009	1.06	0.17

Table 16
(Continued)

M_h ($M_\odot$)	z_ν	ν_{obs} (GHz)	$\Delta\nu_{obs}$ (kHz)	τ_ν 10^{-9}	$\delta T_{b2}^{(th)}$ (10^{-12} K)	$\delta F^{(th)}$ (10^{-12} Jy)	$\delta T_{b2}^{(rs)}$ (10^{-12} K)	$\delta F^{(rs)}$ (10^{-12} Jy)
5.30×10^9	30.41	85.2	0.70	225.0	428.0	7.44	3570.0	62.1
		170	1.40	123.0	53.2	3.68	1170.0	80.9
	25.15	102	0.73	317.0	284.0	7.48	4240.0	112.0
		204	1.45	122.0	22.9	2.40	798.0	83.5
	19.90	128	0.76	428.0	145.0	6.41	4420.0	195.0
		255	1.51	99.3	60.8	1.07	356.0	62.3
	14.65	171	0.78	312.0	25.9	2.25	2060.0	179.0
		341	1.56	32.3	0.34	0.12	38.6	13.4
	9.41	257	0.82	125.0	0.90	0.21	305.0	72.3
		512	1.63	2.74	0.001	0.0009	0.29	0.27

Note. The values with (th) are related to the thermal emission, and the values with (rs) are related to the resonant scattering.

ORCID iDs

V. Shulga ⓘ https://orcid.org/0000-0001-6529-5610

References

Barkana, R., & Loeb, A. 2001, PhR, 349, 125
Basu, K. 2007, NewAR, 51, 431
Bowman, J. D., Rogers, A. E. E., Monsalve, R. A., et al. 2018, Natur, 555, 67
Bromm, V., & Yoshida, N. 2011, ARA&A, 49, 373
Carroll, S. M., Press, W. H., & Turner, E. L. 1992, ARA&A, 30, 499
Chen, R., & McKeever, S. W. 1997, Theory of Thermoluminescence and Related Phenomena (Singapore: World Scientific)
de Bernardis, P., Dubrovich, V., Encrenaz, P., et al. 1993, A&A, 269, 1
Dubrovich, V., Bajkova, A., & Khaikin, V. B. 2008, NewA, 13, 28
Dubrovich, V. K. 1977, SvAL, 3, 128
Eisenstein, D. J., & Hu, W. 1998, ApJ, 496, 605
Fan, X., Carilli, C. L., & Keating, B. 2006, ARA&A, 44, 415
Field, G. B., Somerville, W. B., & Dressler, K. 1966, ARA&A, 4, 207
Flower, D. R. 1997, MNRAS, 288, 627
Flower, D. R., & Pineau des Forêts, G. 2000, MNRAS, 316, 901
Flower, D. R., & Roueff, E. 1998, JPhB, 31, 955
Flower, D. R., & Roueff, E. 1999, MNRAS, 309, 833
Furlanetto, S. R., Oh, S. P., & Briggs, F. H. 2006, PhR, 433, 181
Gosachinskij, I. V., Dubrovich, V. K., Zhelenkov, S. R., Il'in, G. N., & Prozorov, V. A. 2002, ARep, 46, 543
Goss, W. M., & Field, G. B. 1968, ApJ, 151, 177
Iliev, I. T., Shapiro, P. R., Ferrara, A., & Martel, H. 2002, ApJL, 572, L123
Kamaya, H., & Silk, J. 2002, MNRAS, 332, 251
Kamaya, H., & Silk, J. 2003, MNRAS, 339, 1256
Lang, K. R. 1974, Astrophysical Formulae. A. Compendium for the Physicist and Astrophysicist (Berlin: Springer)
Lique, F. 2015, MNRAS, 453, 810
Lique, F., Honvault, P., & Faure, A. 2012, JChPh, 137, 154304
Maoli, R., Ferrucci, V., Melchiorri, F., & Tosti, D. 1996, ApJ, 457, 1
Maoli, R., Melchiorri, F., & Tosti, D. 1994, ApJ, 425, 372
Mizusawa, H., Omukai, K., & Nishi, R. 2005, PASJ, 57, 951
Novosyadlyj, B., Shulga, V., Han, W., Kulinich, Yu., & Tsizh, M. 2018, ApJ, 865, 38
Novosyadlyj, B., Tsizh, M., & Kulinich, Yu. 2016, GReGr, 48, 30
Núñez-López, R., Lipovka, A., & Avila-Reese, V. 2006, MNRAS, 369, 2005
Omukai, K., & Kitayama, T. 2003, ApJ, 599, 738
Persson, C. M. R., Maoli, R., Encrenaz, P., et al. 2010, A&A, 515, A72
Planck Collaboration, Aghanim, N., Akrami, Y., Ashdown, M., et al. 2018a, arXiv:1807.06209
Planck Collaboration, Akrami, Y., Arroja, F., Ashdown, M., et al. 2018b, arXiv:1807.06205
Pritchard, J. R., & Loeb, A. 2012, RPPh, 75, 086901
Purcell, E. M. 1952, ApJ, 116, 457
Rogers, A. E. E., & Barrett, A. H. 1968, ApJ, 151, 163
Roueff, E., & Flower, D. R. 1999, MNRAS, 305, 353
Takayanagi, K. 1963, PThPS, 25, 1
Takayanagi, K., & Nishimura, S. 1960, PASJ, 12, 77
Wrathmall, S. A., Gusdorf, A., & Flower, D. R. 2007, MNRAS, 382, 133